

# Oxygen migration enthalpy likely limits oxide precipitate dissolution during tabula rasa

E. E. Looney, H. S. Laine, A. Youssef, M. A. Jensen, V. LaSalvia, P. Stradins, and T. Buonassisi

Citation: *Appl. Phys. Lett.* **111**, 132102 (2017); doi: 10.1063/1.4987144

View online: <http://dx.doi.org/10.1063/1.4987144>

View Table of Contents: <http://aip.scitation.org/toc/apl/111/13>

Published by the [American Institute of Physics](#)

---

## Articles you may be interested in

[Photo-physical properties of He-related color centers in diamond](#)  
Applied Physics Letters **111**, 111105 (2017); 10.1063/1.4996825

[Characterization of metal fatigue by optical second harmonic generation](#)  
Applied Physics Letters **111**, 131901 (2017); 10.1063/1.4995694

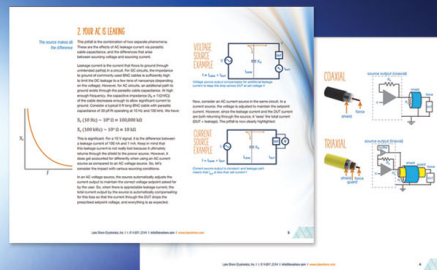
[How nanobubbles lose stability: Effects of surfactants](#)  
Applied Physics Letters **111**, 131601 (2017); 10.1063/1.5000831

[Rectifying and ultraviolet photovoltage characteristics of  \$\text{La}\_{0.9}\text{Na}\_{0.1}\text{MnO}\_3/\text{SrTiO}\_3\text{-Nb}\$  heterostructures](#)  
Applied Physics Letters **111**, 132101 (2017); 10.1063/1.4992010

[Molecular beam epitaxial growth and characterization of AlN nanowall deep UV light emitting diodes](#)  
Applied Physics Letters **111**, 101103 (2017); 10.1063/1.4989551

[Single walled carbon nanotube-based stochastic resonance device with molecular self-noise source](#)  
Applied Physics Letters **111**, 133501 (2017); 10.1063/1.4986812

---



## 5 Electronic Measurement Pitfalls to Avoid

Get the whitepaper

## Oxygen migration enthalpy likely limits oxide precipitate dissolution during *tabula rasa*

E. E. Looney,<sup>1</sup> H. S. Laine,<sup>1,2</sup> A. Youssef,<sup>1</sup> M. A. Jensen,<sup>1</sup> V. LaSalvia,<sup>3</sup> P. Stradins,<sup>3</sup> and T. Buonassisi<sup>1</sup>

<sup>1</sup>Mechanical Engineering Department, Massachusetts Institute of Technology, Cambridge, Massachusetts 02139, USA

<sup>2</sup>Department of Electronics and Nanoengineering, Aalto University, 02150 Espoo, Finland

<sup>3</sup>National Renewable Energy Laboratory, Golden, Colorado 80401, USA

(Received 8 June 2017; accepted 11 September 2017; published online 25 September 2017)

In industrial silicon solar cells, oxygen-related defects lower device efficiencies by up to 20% (rel.). In order to mitigate these defects, a high-temperature homogenization anneal called *tabula rasa* (TR) that has been used in the electronics industry is now proposed for use in solar-grade wafers. This work addresses the kinetics of *tabula rasa* by elucidating the activation energy governing oxide precipitate dissolution, which is found to be  $2.6 \pm 0.5$  eV. This value is consistent within uncertainty to the migration enthalpy of oxygen interstitials in silicon, implying TR to be kinetically limited by oxygen point-defect diffusion. This large activation energy is observed to limit oxygen precipitate dissolution during standard TR conditions, suggesting that more aggressive annealing conditions than conventionally used are required for complete bulk microdefect mitigation. *Published by AIP Publishing.* [<http://dx.doi.org/10.1063/1.4987144>]

The capital expenditure (capex) required to grow the photovoltaics industry is a central barrier to the rapid adoption of solar technologies needed to meet climate targets.<sup>1</sup> One strategy to reduce capex is to increase manufacturing yields. The majority (35%–40%) of industrial monocrystalline silicon for solar cells is made using the Czochralski (Cz) method.<sup>2</sup> About one quarter of the wafers from a typical Cz ingot are affected by oxygen-related “ring” or “swirl” defects that result in up to 20% (rel.) and 4% (abs.) reduction in conversion efficiency after cell processing.<sup>3</sup> Wafers afflicted with these oxygen-related defects are sorted out as a low-quality materials and are either sold at a lower price or scrapped as yield loss. The “swirl” defects, which take their name from their appearance in photoluminescence images, are in reality several types of bulk microdefects (BMDs) that are caused by the interplay of silicon interstitials, vacancies, and oxygen point defects during the solidification of the silicon ingot.<sup>4–7</sup> The final grown-in defect distributions of these swirl defects are described kinetically through the ratio of the pull rate ( $V$ ) to the temperature gradient ( $G$ ) in the radial direction at the interface between the solidified silicon and the melt. When  $V/G$  is above a critical ratio, the crystal is in the vacancy-rich regime, and in a portion of this regime at moderate vacancy supersaturation, oxygen clusters are likely to form in swirl patterns.<sup>8</sup>

Oxygen is the most abundant impurity in Cz-Si, usually present at 10–20 ppma in solar cell materials. Oxygen in silicon takes several forms, from interstitial oxygen with low recombination activity to strained oxide precipitates with high recombination activity.<sup>9,10</sup> During cell fabrication, high-temperature process steps including phosphorus diffusion gettering and thermal oxidation allow oxygen to change between these different morphologies and therefore alter the recombination activity.<sup>6,11,12</sup> To maximize the performance

of Cz-Si solar cells, process engineers must determine which processes leave oxygen in the least harmful form. For  $n$ -type Cz-Si, interstitial oxygen is the least harmful state, and for  $p$ -type Cz-Si, the boron-oxygen degradation mechanism complicates which oxygen morphology is the best as greater interstitial oxygen can increase boron-oxygen degradation. Even though adding oxygen in the interstitial form can be temporarily harmful to  $p$ -type cells, large oxygen precipitates that are recombination centers and internal gettering sites and have a long dissolution time have worse problems in efficiency if present. Therefore, *tabula rasa* (TR) would always aim to completely dissolve all oxygen precipitates and nucleation sites in the interstitial form.<sup>13,14</sup>

One proposed process to mitigate these defects is called *tabula rasa* (TR), which involves rapidly heating the silicon wafer to 1000–1250 °C, holding for a short time up to several minutes, then removing the wafer, and cooling in ambient room temperature.<sup>15,16</sup> In the integrated circuit (IC) industry, this process is used to install a certain vacancy profile in the wafer, while erasing its thermal history, leaving as-grown wafers “blank slates” with respect to oxygen.<sup>17–19</sup> The solar industry currently does not incorporate such an anneal before cell processing, leaving as-grown defects that formed during the crystallization process to evolve throughout the high-temperature process steps of cell fabrication. Some research has been done exploring a similar short high-temperature anneal to mitigate the effects of iron precipitates in different c-Si substrates.<sup>20–23</sup> It has been shown experimentally that harmful ring defects can be erased by an optimized TR process,<sup>7,24–26</sup> and while the growth kinetics of oxygen precipitates are well explored due to their usefulness as internal gettering sites in the IC industry,<sup>27–31</sup> the dissolution kinetics of oxygen precipitates have not been studied in detail experimentally. Through this work, we determine the most likely energy limiting step in the oxygen dissolution process, and

the effectiveness of the TR process is discussed within the context of current knowledge of oxygen precipitate dissolution.<sup>7,10,11</sup> This new knowledge can be utilized in future work in a simplified kinetic model such as the Impurity to Efficiency calculator.<sup>12</sup> With this knowledge, crystal growers and solar cell process engineers are more capable of mitigating oxygen rings effectively, thus improving the PV manufacturing yield.

There are several concerns with the TR process. First, harmful metal impurities can be gettered to and precipitated at oxygen clusters.<sup>32,33</sup> It is essential for the TR process that oxygen-cluster gettering sites are completely dissolved so that metal impurities can then be effectively gettered to the emitter during phosphorus diffusion gettering.<sup>34–36</sup> This leads to the second concern with the TR process: the difficulty in predicting when oxygen precipitates will fully dissolve. Jensen *et al.* tested the TR process on wafers grown by the non-contact crucible method.<sup>37,38</sup> The ring defects observed in photoluminescence images and hypothesized to be related to a high oxygen content in the wafers were not completely removed by the process. Given these concerns, to be an industrially viable process, it is necessary to optimize the TR process for wafers of known oxygen content and distribution to ensure complete dissolution. Using a predictive process model and oxygen characterization techniques, the TR process can be designed that will reliably dissolve oxygen precipitates back into the interstitial form. In this work, we aim to quantify the dissolution kinetics of the TR process to determine the limiting mechanism, whether it is the energy barrier for one oxygen atom to detach from a precipitate or the diffusion (via migration enthalpy) of oxygen atoms moving away from the precipitates through the silicon crystal lattice.

The samples used in these experiments are 745  $\mu\text{m}$  thick, *p*-type, double-side polished, electronic-grade Cz-Si wafers with a resistivity in the range of 10–12  $\Omega\text{ cm}$ . The wafers contain negligible extrinsic impurities other than a total oxygen concentration of 13.8 ppma. These wafers are laser cut into  $3.5 \times 3.5\text{ cm}^2$  rectangles and chemically cleaned for metal and organic contaminants. Each sample then undergoes a series of high-temperature steps to nucleate and grow large oxygen precipitates in a spatially homogeneous pattern.<sup>19,39</sup> These growth steps are done under an  $\text{N}_2$  atmosphere in a quartz tube furnace. The time-temperature profile used to grow oxygen precipitates includes a nucleation step at 650  $^\circ\text{C}$  for 6 h, precipitate growth steps at 800  $^\circ\text{C}$  for 4 h, 925  $^\circ\text{C}$  for 4 h, and 1000  $^\circ\text{C}$  for 16 h, and finally cooling to 700  $^\circ\text{C}$  in the furnace before being pulled out of the furnace to cool in ambient. The ramp rate is 10  $^\circ\text{C}/\text{min}$ . The samples are then cleaved into smaller  $1 \times 1\text{ cm}^2$  pieces and chemically etched with CP4 and HF-dipped to remove any surface contamination or oxide left from the high-temperature processing.

A series of TR processes are performed on the samples at five temperatures between 1100  $^\circ\text{C}$  and 1290  $^\circ\text{C}$ . For each temperature, TR experiments were performed at six different times between 1 and 30 min. We expect the highest temperature and longest time TR process (1290  $^\circ\text{C}$  for 30 min) to most effectively dissolve grown-in oxygen precipitates and the shortest time and lowest temperature

process (1100  $^\circ\text{C}$  for 1 min) to dissolve the precipitates the least. The TR process is done in a horizontal mullite tube furnace, under an  $\text{N}_2$  atmosphere, with temperatures measured using external thermocouples and a disappearing filament optical pyrometer targeted at a silicon base plate on which the samples are placed. The push and pull times both into and out of the preheated furnace were 10 s, and the samples were placed at the end of the furnace for 10 s before being placed on a large silicon heat sink and cooled in ambient air. The samples were then HF dipped to remove any oxide formed on the surface.

The oxygen content in the wafer was characterized by Fourier transform infrared spectroscopy (FTIR) and chemical etching to reveal defects. FTIR at room temperature was used to determine the interstitial oxygen ( $\text{O}_i$ ) concentration at 1107  $\text{cm}^{-1}$  before precipitate growth, after precipitate growth, and after the TR step. These measurements were calibrated using ASTM standard 121–83. A defect etch on a control wafer performed before oxygen growth revealed no etch pits (not shown). Hence, all oxygen was assumed to be in the interstitial form, and the FTIR measurement reveals the total oxygen content. This was also confirmed by measuring the as-received sample, annealing it for 18 h at 1290  $^\circ\text{C}$  to be certain that all oxygen was dissolved, and re-measuring to show an equivalent amount of interstitial oxygen. FTIR showed that  $[\text{O}_i]$  in this sample was indeed the same after the anneal as before the anneal at 13.8 ppma or  $6.9 \times 10^{17}$  atoms/ $\text{cm}^3$ . After growth,  $[\text{O}_i]$  dropped to 5.4 ppma, indicating that 61% of oxygen atoms precipitated during growth. Through chemical defect etching done for 45 s ( $\text{HF}:\text{CH}_3\text{COOH}:\text{HNO}_3$  with a volume ratio of 36:15:2),<sup>40</sup> the precipitate density is determined to be around  $2.6 \times 10^9$  ppt/ $\text{cm}^3$ . These precipitate sizes are quantified with the volumetric density determined from the etch rate measured to be 16.8  $\mu\text{m}/\text{min}$ . Assuming a  $\text{SiO}_2$ ,  $\alpha$ -quartz chemical state with a bond length of  $1.6 \times 10^{-8}\text{ cm}$  in a hexagonal pattern and also assuming that these precipitates are all of similar size, the oxygen precipitates have an average diameter between 55 and 65 nm or an average of  $1\text{--}2 \times 10^8$  oxygen atoms per precipitate. It is noted that oxygen precipitates grow in a distribution of sizes based on the free energy of precipitate formation during nucleation and growth, and so, these reported sizes are averages only.<sup>27</sup> Finally, after each TR step, FTIR and defect etching are performed again to determine how many of these precipitates have dissolved into interstitial oxygen. To confirm that re-precipitation does not occur during the cool down after the process, a sample at each temperature for the 30-min process was directly quenched in silicone oil. Using these methods, the oxygen distribution is comprehensively characterized, including the density of interstitial and precipitated oxygen as well as precipitate size and density.

Figure 1 shows plots  $[\text{O}_i]$  as a function of annealing time for each TR temperature. As expected, the interstitial oxygen concentration increases steadily with the increasing TR temperature, which increases the oxygen solid solubility and causes more precipitates to dissolve. To quantify the dependence of the dissolution rate on TR temperature, the dissolution time constant,  $\tau_{\text{diss}}$ , is determined for each temperature through the following equation:

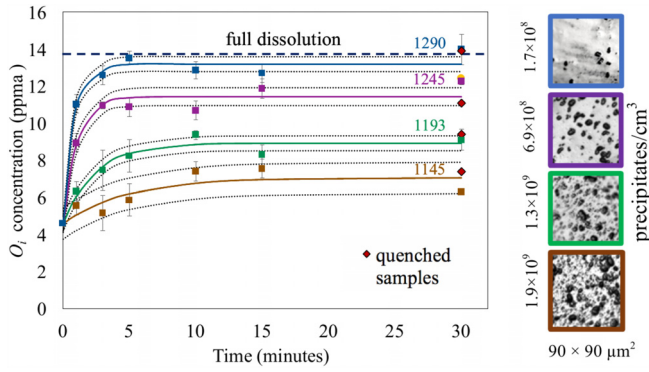


FIG. 1. Dissolution curves plotted as the interstitial oxygen content for four temperatures and six times. The dissolution time constant ranged from around 1–6 min between the temperatures, and none of the processes completely dissolved the precipitates. Also shown are samples at each temperature quenched in silicone oil. At right, defect etch images of the  $90 \times 90 \mu\text{m}^2$  area show the decreasing density of oxygen precipitates (displayed below each image) at each temperature for the 30-min anneal with quenching. The dashed lines represent 85% confidence intervals calculated from the error in the free parameter, final concentration at the last time step. The error bars represent the standard error due to the distribution of measurements taken at each time step. If only one measurement was taken at a time step, the error bars are an average of all standard error.

$$[O_i](t) \propto C_f \left[ 1 - \exp\left(-\frac{t}{\tau_{diss}}\right) \right], \quad (1)$$

where  $C_f$  is the observed final concentration of interstitial oxygen at each TR temperature. The fitted lines are plotted in Fig. 1 (solid lines).

The four curves plotted represent the four TR process temperatures and demonstrate the dissolution of oxygen precipitates at a steep initial rate as the high density of smaller precipitates quickly dissolve reaching a steady state as the larger precipitates dissolve more slowly. No re-precipitation occurs during cool down, as demonstrated by the quenched samples in Fig. 1. The solid solubility limit of interstitial oxygen in silicon is not achieved during the longest 30-min TR run for any of these temperatures except for the



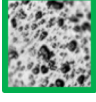
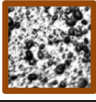

1145 °C curve using the intrinsic solubility of interstitial oxygen in silicon described by  $9 \times 10^{22} \exp\left(\frac{-1.52 \text{ eV}}{k_B T}\right) \text{ cm}^{-3}$ .<sup>41</sup>

At 1193 °C, 1245 °C, and 1290 °C,  $[O_i]$  reaches a very slow, steady dissolution rate below its solid solubility limits, and based on first principles, it will eventually reach the solubility limit at that temperature, just slowly due to the process being kinetically limited. The single exponential model captures the early dissolution at these TR temperatures but does not capture dissolution at longer times as lower density, larger precipitates continue to dissolve. Incorporating dissolution models based on inhomogeneous precipitate size dissolution is a good next step for the model to incorporate dissolution at all temperatures for all sizes of precipitates. Table I displays the experimental parameters and solubility limits of interstitial oxygen for each 30-min process at all four temperatures.

Etch pit images are shown in the right of the dissolution curves corresponding to a 30-min TR process at each temperature and silicone oil quench. The density of precipitates decreases at each higher temperature, showing the dissolution of a certain percentage of oxygen precipitates. In each sample, the density of precipitates and the interstitial oxygen content are measured and used to calculate the precipitate radius which is found to not vary drastically between temperatures. As can be seen in Fig. 1, precipitates do not fully dissolve for any of the TR experiments. The precipitate density ranges between  $1 \times 10^8$  and  $7 \times 10^8$  precipitates/ $\text{cm}^3$ , the interstitial oxygen concentration between  $3.7 \times 10^{17}$  and  $6.8 \times 10^{17}$  atoms/ $\text{cm}^3$ , and the average precipitate radii between 45 and 60 nm. The highest temperature TR process at 1290 °C results in the lowest precipitate density and the highest interstitial oxygen content, whereas the lowest TR temperature at 1145 °C results in a lower interstitial oxygen content and higher precipitate density.

The activation energy for dissolution,  $E_a$ , was found using the fitted dissolution time constants,  $\tau_{diss}$ , and fitting these to an Arrhenius-type temperature-dependent equation

TABLE I. Experimental parameters. Total interstitial oxygen content = 13.75 ppma,  $6.9 \times 10^{17}$  atoms/ $\text{cm}^3$ .

Temperature °C	Precipitate density		Final interstitial oxygen from fit		Solubility limit	
	ppt/ $\text{cm}^3$		oxygen atoms/ $\text{cm}^3$	ppma	oxygen atoms/ $\text{cm}^3$	ppma
1290	$1.7 \times 10^8$		$6.6 \times 10^{17}$	13.2	$1.1 \times 10^{18}$	22.6
1245	$6.9 \times 10^8$		$5.7 \times 10^{17}$	11.4	$8.1 \times 10^{17}$	16.2
1193	$1.3 \times 10^9$		$4.5 \times 10^{17}$	8.9	$5.4 \times 10^{17}$	10.7
1145	$1.9 \times 10^9$		$3.5 \times 10^{17}$	7.0	$3.6 \times 10^{17}$	7.1

$$\frac{1}{\tau_{\text{diss}}} \propto \exp\left(\frac{E_a}{k_B T}\right). \quad (2)$$

The activation energy indicates the limiting physical process in dissolution within the error of the measurement and fit. This could be, for example, the reaction in which one or more oxygen atoms detach from a precipitate (reaction-limited dissolution), as has been observed for dissolution of iron-silicide precipitates.<sup>42</sup> If the activation energy is found to be close to the migration enthalpy of interstitial oxygen in silicon, the diffusion of an oxygen atom away from a precipitate is the energy-limiting step and no extra energy is needed to dissolve precipitates greater than the kinetic limitations of diffusion.<sup>43</sup> If the activation energy is smaller than the migration enthalpy, the dissolution of oxygen precipitates is somehow enhanced, lowering the energy needed for oxygen to diffuse away from a precipitate. As can be seen in Fig. 2, the activation energy was found to be  $2.6 \pm 0.5$  eV, within the range of migration enthalpies for  $[O_i]$  in silicon ( $2.53 \pm 0.3$  eV).<sup>41</sup>

The dissolution of oxide precipitates in these samples appears to be kinetically (diffusion) limited as opposed to solubility limited. Further evidence supporting this hypothesis is the fact that the measured  $[O_i]$  concentration in Fig. 1 never reaches the total oxygen concentration, despite the annealing temperature resulting in a solubility limit above the total oxygen concentration in three out of the four anneals. The plateaus observed in Fig. 1 can be understood assuming a bimodal distribution of the oxide precipitate size, consistent with literature reports<sup>27,44–46</sup> and the optical microscopy observation of residual bulk microdefects at the end of the anneals (Fig. 1, inset). The initial (fast) rise in interstitial oxygen concentration in Fig. 1 can be attributed to both a solubility enhancement during dissolution and orders of magnitude larger numbers of small precipitates, while the dissolution of fewer larger precipitates is more strongly affected by the large migration enthalpy of oxygen. This results in the apparent plateau of interstitial oxygen concentration at longer times in Fig. 1. If correct, this hypothesis

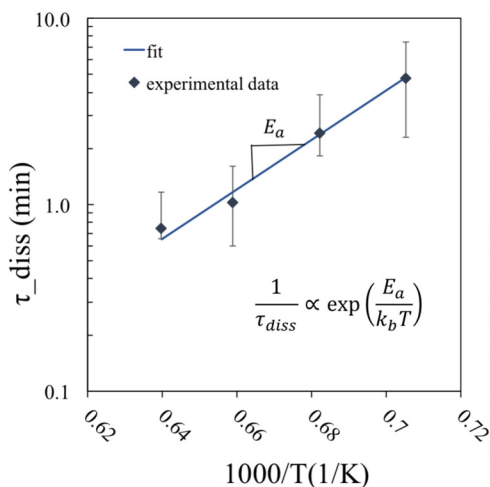


FIG. 2. Dissolution time constant plotted as a function of inverse temperature. An activation energy of  $2.6 \pm 0.5$  eV was found with an Arrhenius-like temperature dependent dissolution behavior. The error bars represent confidence in the dissolution time constant fit from Fig. 1.

implies that with longer annealing time and/or higher temperature, the larger precipitates would more fully dissolve, indicating that further optimization of TR for these samples is necessary to mitigate all oxygen-related defects.

The TR anneal used in the electronics industry would likely not be adequate for solar-grade silicon. The typical TR process used in the electronics industry between 1000 and 1250 °C for 1–5 min would not be sufficient for our samples because of the large oxide precipitate size and the large dissolution energy barrier. The samples used in these experiments have oxygen precipitates with an average radius of around 30 nm, which is larger than those typically present in IC- and solar-grade CZ.<sup>5</sup> This does not change the results of kinetically limited dissolution but makes the times and temperatures to dissolve longer in this experiment than that would be needed for most Cz-Si cells. However, precipitates over 30 nm have been found in as-grown multicrystalline silicon for solar cells, providing insight into the process parameters that may be necessary for TR to work on other commonly used solar materials.<sup>47–50</sup> Therefore, TR times and temperatures must be carefully chosen and tailored to the as-grown oxygen content and morphologies for a particular material to ensure repeatable success in dissolving/suppressing precipitates. Longer times and higher temperatures may be required to fully dissolve all oxygen nucleation sites and precipitates than conventionally used.

In conclusion, *tabula rasa* is a promising solution to overcome oxygen-related defects in solar-grade silicon materials. To ensure maximum process efficacy and minimal cost, optimal processing conditions must be found. This work shows that the activation energy of oxygen-related defect dissolution is in the same range as the oxygen interstitial migration enthalpy,  $\sim 2.6$  eV, suggesting TR to be limited by oxygen diffusion. Consequently, TR may need to incorporate longer times and higher temperatures than previously used in the literature, as determined by the size and density of the oxygen precipitates in addition to total oxygen concentration, within the as-grown wafer. Quantification of oxygen dissolution in silicon in this study opens a way to optimize through simulation TR time-temperature profiles to mitigate the recombination activity of oxygen-related defects in Cz-Si PV-relevant materials.

The authors thank Bob Standley at MEMC for insightful discussions, Arthur McClelland at the Center for Nanoscale Systems for spectroscopy expertise, Jim Serdy for help in constructing the TR setup, and Zhe Liu for helpful discussions and guidance during the paper-writing process. This material is based upon work supported by the U.S. National Science Foundation (NSF) and the U.S. Department of Energy (DOE) under NSF CA No. EEC-1041895 and U.S. DOE EERE Contract SETP DE-EE00030301 (SuNLaMP). H.S.L. thanks the Fulbright Technology Industries of Finland Grant. E.E.L. and M.A.J. acknowledge support by the NSF Graduate Research Fellowship under Grant No. 1122374.

<sup>1</sup>D. B. Needleman, J. R. Poindexter, R. C. Kurchin, I. M. Peters, and T. Buonassisi, *Energy Environ. Sci.* **9**, 2122 (2016).

<sup>2</sup>A. Metz, *International Technology Roadmap for Photovoltaic (ITRPV) 2014 Results* (VDMA, Inc., 2015).

- <sup>3</sup>J. Haunschild, I. E. Reis, J. Geilker, and S. Rein, *Phys. Status Solidi - Rapid Res. Lett.* **5**, 199 (2011).
- <sup>4</sup>J. D. Murphy, K. Bothe, R. Krain, V. V. Voronkov, and R. J. Falster, *J. Appl. Phys.* **111**, 113709 (2012).
- <sup>5</sup>A. Le Donne, S. Binetti, V. Folegatti, and G. Coletti, *Appl. Phys. Lett.* **109**, 033907 (2016).
- <sup>6</sup>J. Schön, A. Youssef, S. Park, L. E. Mundt, T. Niewelt, S. Mack, K. Nakajima, K. Morishita, R. Murai, M. A. Jensen, T. Buonassisi, M. C. Schubert, A. Youssef, S. Park, L. E. Mundt, T. Niewelt, T. Buonassisi, and M. C. Schubert, *J. Appl. Phys.* **120**, 105703 (2016).
- <sup>7</sup>A. Youssef, J. Schon, T. Niewelt, S. Mack, S. Park, K. Nakajima, K. Morishita, R. Murai, M. A. Jensen, T. Buonassisi, and M. C. Schubert, in *43rd IEEE Photovoltaic Specialist Conference Proceeding* (2016).
- <sup>8</sup>V. V. Voronkov and R. Falster, *J. Cryst. Growth* **204**, 462 (1999).
- <sup>9</sup>J. Michel and L. C. Kimmerling, *Semicond. Semimetals* **42**, 251–284 (1994).
- <sup>10</sup>J. D. Murphy, K. Bothe, R. Krain, M. Olmo, V. V. Voronkov, and R. J. Falster, *Solid State Phenom.* **178–179**, 205 (2011).
- <sup>11</sup>J. Schön, V. Vähänissi, A. Haarahiltunen, M. C. Schubert, W. Warta, and H. Savin, *J. Appl. Phys.* **116**, 244503 (2014).
- <sup>12</sup>M. Syre, S. Karazhanov, B. R. Olaisen, A. Holt, and B. G. Svensson, *J. Appl. Phys.* **110**, 024912 (2011).
- <sup>13</sup>J. Schmidt and K. Bothe, *Phys. Rev. B* **69**, 024107 (2004).
- <sup>14</sup>B. Lim, K. Bothe, and J. Schmidt, *J. Appl. Phys.* **107**, 123707 (2010).
- <sup>15</sup>R. J. Falster, M. Cornara, D. Gambaro, M. Olmo, and M. Pagani, *Solid State Phenom.* **57–58**, 123 (1997).
- <sup>16</sup>F. Roozeboom, E. Gusev, L. J. Chen, M. C. Ozturk, D. L. Kwong, and P. J. Timans, in *Electrochemical Society Proceedings* (2003).
- <sup>17</sup>G. Kissinger, J. Dabrowski, a. Sattler, C. Seuring, T. Müller, H. Richter, and W. von Ammon, *J. Electrochem. Soc.* **154**, H454 (2007).
- <sup>18</sup>R. Falster and V. V. Voronkov, *Mater. Sci. Eng. B* **73**, 87 (2000).
- <sup>19</sup>R. Falster, *Futur. Fab Int.* **12**, 240 (2002).
- <sup>20</sup>Z. Liu, V. Vahanissi, H. S. Laine, M. Lindeber, M. Yli-Koshi, and H. Savin, *Adv. Electron. Mater.* **3**, 1600435 (2017).
- <sup>21</sup>V. Osinniy, A. Nylandsted Larsen, E. Hvidsten Dahl, E. Enebak, A. K. Sjøiland, R. Tronstad, and Y. Safir, *Sol. Energy Mater. Sol. Cells* **101**, 123 (2012).
- <sup>22</sup>P. S. Plekhanov, R. Gafiteanu, U. M. Gosele, and T. Y. Tan, *J. Appl. Phys.* **86**, 2453 (1999).
- <sup>23</sup>M. Di Sabatino, S. Binetti, J. Libal, M. Acciarri, H. Nordmark, and E. J. Øvrelid, *Sol. Energy Mater. Sol. Cells* **95**, 529 (2011).
- <sup>24</sup>V. LaSalvia, M. A. Jensen, A. Youssef, W. Nemeth, M. Page, T. Buonassisi, and P. Stradins, in *43rd IEEE Photovoltaic Specialist Conference Proceeding* (2016), p. 1047.
- <sup>25</sup>B. Sopori, S. Devayajanam, P. Basnyat, T. Tan, A. Upadhyaya, A. Rohatgi, N. Renewable, and G. T. A. Technologies, *J. Photovolt.* **7**, 97 (2017).
- <sup>26</sup>F. E. Rougieux, H. T. Nguyen, D. H. Macdonald, B. Mitchell, and R. Falster, *IEEE J. Photovolt.* **7**, 735 (2017).
- <sup>27</sup>B. Trzynadlowski, *Reduced Moment-Based Models for Oxygen Precipitates and Dislocation Loops in Silicon* (University of Washington, 2013).
- <sup>28</sup>S. Senkader, J. Esfandyari, and G. Hobler, *J. Appl. Phys.* **78**, 6469 (1995).
- <sup>29</sup>B. G. Ko and K. D. Kwack, *J. Appl. Phys.* **85**, 2100 (1999).
- <sup>30</sup>K. Sueoka, M. Akatsuka, M. Okui, and H. Katahama, *J. Electrochem. Soc.* **150**, G469 (2003).
- <sup>31</sup>A. Haarahiltunen, H. Väinölä, O. Anttila, M. Yli-Koski, and J. Sinkkonen, *J. Appl. Phys.* **101**, 043507 (2007).
- <sup>32</sup>W. Seifert, M. Kittler, M. Seibt, and A. Buczkowski, *Solid State Phenom.* **47–48**, 365 (1996).
- <sup>33</sup>J. D. Murphy, R. E. McGuire, K. Bothe, V. V. Voronkov, and R. J. Falster, *J. Appl. Phys.* **116**, 053514 (2014).
- <sup>34</sup>D. P. Fenning, A. S. Zuschlag, M. I. Bertoni, B. Lai, G. Hahn, and T. Buonassisi, *J. Appl. Phys.* **113**, 214504 (2013).
- <sup>35</sup>A. E. Morishige, M. A. Jensen, J. Hofstetter, P. X. T. Yen, C. Wang, B. Lai, D. P. Fenning, and T. Buonassisi, *Appl. Phys. Lett.* **108**, 202104 (2016).
- <sup>36</sup>A. E. Morishige, H. S. Laine, J. Schon, A. Haarahiltunen, J. Hofstetter, C. del Canizo, M. C. Schubert, H. Savin, and T. Buonassisi, *Appl. Phys. A: Mater. Sci. Process.* **120**, 1357 (2015).
- <sup>37</sup>K. Nakajima, K. Morishita, and R. Murai, *J. Cryst. Growth* **405**, 44 (2014).
- <sup>38</sup>M. A. Jensen, V. LaSalvia, A. E. Morishige, K. Nakajima, Y. Veschetti, F. Jay, A. Jouini, A. Youssef, and P. Stradins, *Energy Procedia* **92**, 815 (2016).
- <sup>39</sup>K. F. Kelton, R. Falster, D. Gambaro, M. Olmo, M. Cornara, and P. F. Wei, *J. Appl. Phys.* **85**, 8097 (1999).
- <sup>40</sup>B. L. Sopori, *J. Electrochem. Soc. Solid-State Sci. Technol.* **131**, 667 (1984).
- <sup>41</sup>J. C. Mikkelsen, *Mater. Res. Symp. Proc.* **59**, 19–30 (1985).
- <sup>42</sup>P. Zhang, H. Väinölä, A. A. Istratov, and E. R. Weber, *Appl. Phys. Lett.* **83**, 4324 (2003).
- <sup>43</sup>F. Shimura, *Appl. Phys. Lett.* **39**, 987 (1981).
- <sup>44</sup>P. Fraundorf, G. K. Fraundorf, and F. Shimura, *J. Appl. Phys.* **58**, 4049 (1985).
- <sup>45</sup>Z. Wang, *Modeling Microdefects Formation in Crystalline Silicon: The Roles of Point Defects and Oxygen* (Massachusetts Institute of Technology, 2002).
- <sup>46</sup>K. Nakashima, K. Nakamura, T. Saishoji, Y. Watanabe, Y. Mitsushima, and N. Inoue, "Observation of ring-OSF nuclei in as-grown CZ silicon crystals by highly selective reactive ion etching," in *High Purity Silicon VII: Proceedings of the International Symposium* (Electrochemical Society, Pennington, N.J., 2002), pp. 82–90.
- <sup>47</sup>M. Rinio, A. Yodyungyong, S. Keipert-Colberg, D. Borchert, and A. Montesdeoca-Santana, *Phys. Status Solidi A* **208**, 760 (2011).
- <sup>48</sup>S. Riepe, I. E. Reis, W. Kwapil, M. A. Falkenberg, J. Schön, H. Behnken, J. Bauer, D. Kreßner-Kiel, W. Seifert, and W. Koch, *Phys. Status Solidi C* **8**, 733 (2011).
- <sup>49</sup>H. J. Möller, C. Funke, A. Lawrenz, S. Riedel, and M. Werner, *Sol. Energy Mater. Sol. Cells* **72**, 403 (2002).
- <sup>50</sup>M. Rinio, *Untersuchung Der Prozessabhängigen Ladungsträgerrekombination an Versetzungen in Siliziumsolarzellen* (Technical University of Mining in Freiberg, 1967).